HHS Public Access

Author manuscript

J Control Release. Author manuscript; available in PMC 2021 December 10.

Published in final edited form as:

J Control Release. 2020 December 10; 328: 276–285. doi:10.1016/j.jconrel.2020.08.053.

Characterization of focused ultrasound-mediated brainstem delivery of intranasally administered agents

Dezhuang Ye[a], **Jingyi Luan**[a], **Hannah Pang**[b], **Yaoheng Yang**[b], **Arash Nazeri**[c], **Joshua B. Rubin**[d,e], **Hong Chen**[b,f,*]

[a]Department of Mechanical Engineering and Materials Science, Washington University in St. Louis, Saint Louis, Missouri, 63130, USA.

[b]Department of Biomedical Engineering, Washington University in St. Louis, Saint Louis, Missouri, 63130, USA

[c]Mallinckrodt Institute of Radiology, Washington University School of Medicine, St. Louis, MO., 63110, USA.

[d]Departments of Pediatrics and Neuroscience, Washington University School of Medicine, St. Louis, Missouri 63110, USA

[e]Department of Neuroscience, Washington University School of Medicine, St. Louis, Missouri 63110, USA

[f]Department of Radiation Oncology, Washington University School of Medicine, Saint Louis, Missouri, 63108, USA.

Abstract

Focused ultrasound-mediated intranasal (FUSIN) delivery is a recently proposed technique that bypasses the blood-brain barrier to achieve noninvasive and localized brain drug delivery. The goal of this study was to characterize FUSIN drug delivery outcomes in mice with regard to its dependency on several critical experimental factors, including the time interval between IN administration and FUS sonication (T_{lag1}), the FUS pressure, and the time for sacrificing the mice post-FUS (T_{lag2}). Wild-type mice were treated by FUSIN delivery of near-infrared fluorescent dye-labeled bovine serum albumin (800CW-BSA, used as a model agent). 800CW-BSA was

[*]**Address correspondence to:** Hong Chen, Ph.D. Department of Biomedical Engineering and Radiation Oncology, Washington University in St. Louis. 4511 Forest Park Ave. St. Louis, MO, 63108, USA. hongchen@wustl.edu.

Credit author statement

Dezhuang Ye: Conceptualization, Methodology, Data Curation, Formal analysis, Investigation, Writing - Original Draft, Visualization;
Jingyi Luan: Resources, Validation, Writing - Review & Edi;
Hannah Pang: Formal analysis, Validation, Writing - Review & Editing;
Yaoheng Yang: Data Curation, Writing - Review & Editing;
Arash Nazeri: Formal analysis, Writing - Review & Editing;
Joshua B. Rubin: Supervision, Writing - Review & Editing;
HongChen: Conceptualization, Resources, Writing - Review & Editing, Visualization, Supervision, Project administration, Funding acquisition.

Competing interests

The authors have declared that no competing interest exists.

intranasally administered to the mice *in vivo,* followed by intravenous injection of microbubbles and FUS sonication at the brainstem. Fluorescence imaging of *ex vivo* mouse brain slices was used to quantify the delivery outcomes of 800CW-BSA. Major organs, along with the nasal tissue and trigeminal nerve, were harvested to assess the biodistribution of 800CW-BSA. The delivery outcome of 800CW-BSA was the highest at the brainstem when T_{lag1} was 0.5 h, which was on average 24.5-fold, 5.4-fold, and 21.6-fold higher than those of the IN only, T_{lag1} = 1.5 h, and T_{lag1} = 4.0 h, respectively. The FUSIN delivery outcome at the lowest pressure level, 0.43 MPa, was on average 1.8-fold and 3.7-fold higher than those at 0.56 MPa and 0.70 MPa, respectively. The mean concentration of 800CW-BSA in the brainstem after FUSIN delivery decreased from 0.5 h to 4.0 h post-FUS. The accumulation of 800CW-BSA was low in the heart, lung, spleen, kidneys, and liver, but high in the stomach and intestines. This study revealed the unique characteristics of FUSIN as a noninvasive, efficient, and localized brain drug delivery technique.

Keywords

Focused ultrasound; Intranasal delivery; Brain drug delivery; Blood-brain barrier; Brainstem

Introduction

Transcranial focused ultrasound (FUS) in combination with microbubbles has been used for noninvasive, localized, and reversible blood-brain barrier (BBB) disruption (FUS-BBBD) to enhance the delivery of intravenously injected drugs to FUS-targeted brain sites [1]. FUS noninvasively penetrates the skull and focuses on a small focal region of millimeter-scale dimensions. Microbubbles, which have been used in the clinic as ultrasound contrast agents for imaging, are administered by intravenous (IV) injection. After IV injection, they are confined to the vasculature due to their relatively large sizes (1–10 μm). Microbubbles amplify and localize FUS-mediated mechanical effects on the vasculature through FUS-induced cavitation (*i.e.*, microbubble expansion, contraction, and collapse), which generates mechanical forces on the vasculature [2] and transiently increases BBB permeability. FUS-BBBD has been used to deliver a wide range of therapeutic agents across the BBB to the brain, such as small molecule drugs [3], protein drugs [4,5], viruses [6–8], and even cells [9,10]. Early phase clinical trials have demonstrated the feasibility and safety of FUS-BBBD in patients with glioblastoma [11–13], Alzheimer's disease [14–16], and amyotrophic lateral sclerosis [17]. Although promising, this technique requires therapeutic agents to be injected through the IV route, which is associated with systemic exposure of the agents to the whole body.

Intranasal (IN) drug delivery provides an alternative route for drug administration to the brain because it is a painless, simple, and noninvasive approach that allows direct agent delivery from the nose to the brain. It bypasses the BBB and eliminates the need for systemic delivery, thereby minimizing associated side effects. IN-administered drugs use two major routes to reach the brain – one through the olfactory nerve to the olfactory bulb, and the other through the trigeminal nerve to the brainstem. Therefore, IN delivery holds a unique advantage, especially for drug delivery to the brainstem. When the administered agents reach the brain entry points, they can be transported along the perivascular space by

the “perivascular pump effect,” which arises from heartbeat-driven pulsation (expansion and contraction) of blood vessel walls [18–20]. IN administration has already been used for the delivery of a wide range of therapeutics to the brain (e.g., peptides [21], proteins [22], gene vectors [23,24], nanoparticles [25,26], and stem cells [27]), not only in animal studies but also in humans [28]. However, two major limitations – low delivery efficiency and lack of disease-site targeting – prevent its broad and successful application in translational research [29,30].

FUS-mediated intranasal (FUSIN) delivery is a recently proposed brain drug delivery technique that capitalizes on the unique advantages of the IN route for direct nose-to-brain drug administration as well as FUS in combination with microbubbles for targeted and enhanced delivery to the brain [31–34]. FUS-induced microbubble cavitation pushes and pulls on the adjacent blood vessel [35], generating the proposed “microbubble pump effect” [33]. The microbubble pump effect may lead to the enhanced penetration and accumulation of IN-administered drugs distributed in the perivascular space. FUSIN was first reported in 2014 and showed improved delivery of dextrans and a protein drug (brain-derived neurotrophic factor) to the FUS-targeted caudate-putamen of mouse brains [31,32]. It was also used to deliver fluorescently labeled gold nanoclusters and radiolabeled gold nanoclusters to the brainstem [33]. A recent study reported that FUSIN delivery of the brain-derived neurotrophic factor produced neuro-restorative effects in a Parkinson’s disease mouse model [34]. All these previous findings suggest that FUSIN is a promising brain drug delivery technique that can locally enhance the delivery efficiency of different agents to various brain regions.

The objective of the current study was to characterize the dependency of FUSIN drug delivery outcome on several critical experimental parameters, including the time interval between IN administration and FUS application, the FUS pressure, and the sampling time (the waiting time after FUS treatment to sacrifice the mouse). We selected fluorescently labeled albumin as the model agent because it has been widely used as a model agent to study protein-drug pharmacokinetics [36,37], and previous studies have used it to quantify the BBB permeability [38,39].

Materials and Methods

Animals and study design

All animal procedures were reviewed and approved by the Institutional Animal Care and Use Committee in accordance with the National Institutes of Health Guidelines for animal research. Cr.NIH (Swiss) mice (6–8 weeks, ~25 g body weight, female) were purchased from Charles River Laboratory (Wilmington, MA, USA). The animals were housed in a room maintained at 22°C and 55% relative humidity, with a 12-h/12-h light/dark cycle and access to standard laboratory chow and water. A total of 48 mice (Table 1) were used to study the dependency of FUSIN delivery outcome on the time interval between IN administration and FUS sonication, the FUS pressure, and the sampling time after FUS treatment. This study followed a one-factor-at-a-time (OFAT) experimental design as the three tested parameters (T_{lag1}, T_{lag2}, and pressure), which represented key experimental

parameters at different stages of the experimental procedures (Fig. 1D), were expected to not interfere with each other. The justifications for the study design are described below.

Based on our previous study [32], FUS treatment applied after IN administration achieved higher delivery efficiency than FUS applied before IN administration. However, the dependency of FUSIN delivery on the time interval between IN and FUS (T_{lag1}, defined as the time interval between the end of IN administration and the beginning of FUS sonication) had not been evaluated. This study chose three different time intervals, T_{lag1} = 0.5 h, 1.5 h, and 4.0 h, in reference to a previous study that reported the pharmacokinetics of IN-delivered albumin in different brain locations [40]. Specifically, it showed that albumin concentration in the pons, which is part of the brainstem, significantly decreased as time increased at these three time points post-IN: 0.5 h, 1.5 h, and 4.0 h. Mice in groups 2 – 4 (Table 1) were used to study the effect of T_{lag1}. The control group (group 1) was administered with 800CW-BSA without FUS. The pressure was selected to be 0.56 MPa because this pressure led to successful and safe FUSIN delivery in our previous reported study [33] and pressure levels at around 0.5 MPa have been shown to be safe for FUS combined with microbubble applications in the mouse brain [46,47].

FUS treatment is controlled by multiple parameters, such as FUS frequency, acoustic pressure, pulse length, pulse repetition frequency, and sonication duration. The peak-negative pressure is a critical parameter, if not the most important one, that is directly related to the microbubble cavitation activities in FUS treatment. The mechanical index (MI) calculated by the peak-negative pressure divided by the square root of the center frequency has been commonly used to predict the likelihood of cavitation. Recently, Bader et al. derived the cavitation index (CI), defined as the peak-negative pressure divided by the center frequency, to gauge the likelihood of subharmonic emissions due to microbubble stable cavitation [41,42]. Moreover, the peak-negative pressure has been found in many previous FUS combined with microbubbles mediated drug delivery studies to have a significant correlation with the drug delivery outcome [43–45]. Therefore, the current study focused on assessing the impact of the peak-negative pressure on FUSIN. Mice in groups 2, 7, and 8 (Table 1) were used to evaluate FUSIN delivery under three acoustic pressure levels centered around 0.56 MPa: 0.43 MPa, 0.56 MPa, and 0.70 MPa. These pressure levels were similar to those commonly used in FUS-BBBD studies [46–48].

In order to examine the pharmacokinetics and clearance of agents delivered by FUSIN, three groups of mice were perfused at different time points post-FUS (T_{lag2}, defined as the time interval between the end of FUS sonication and the beginning of animal sacrifacing procedure). Mice in groups 2, 5, and 6 (Table 1) were used to study the impact of the sampling time: T_{lag2} = 0.5 h, 1.0 h, and 4.0 h. We harvested the mouse brains and other major organs (heart, lung, spleen, kidneys, liver, stomach, intestines) and dissected the nose tissue and trigeminal nerve to evaluate the biodistribution and kinetics of FUSIN-delivered agents.

Near-infrared fluorescent dye-labeled bovine serum albumin (800CW-BSA)

Biotin and 800CW (LI-COR Biosciences, Lincoln, NE) were activated with N-hydroxysuccinimide (NHS) ester and conjugated to the BSA by the amide bond through

EDC/NHS (1-Ethyl-3-(3-dimethylaminopropyl)carbodiimide/N-hydroxysuccinimide) chemistry. The amide bond is one of the most abundant chemical bonds with high stability in various reaction conditions. It widely exists in many organic molecules, including peptides, proteins, DNA and RNA [49]. The EDC/NHS chemistry has been commonly used in both preclinical and clinical studies to label peptides, proteins, and antibodies with near-infrared (NIR) dyes, including 800CW [50–56]. Specifically, in pH 7–9 buffers, NHS esters react efficiently with primary amino groups ($-NH_2$) by the nucleophilic attack, forming an amide bond and releasing the NHS. 2 mg of NHS-activated biotin (NHS-PEG4-Biotin, Thermo Scientific, Prod #: 21329) was added to 2.2 mL of BSA (Sigma-Aldrich, A7030) solution (5 mg/mL in 1× PBS). The mixture was incubated at room temperature (~22°C) for 1 hour to complete the reaction. Excess NHS-PEG4-Biotin was removed from the solution using a desalting column (5 mL, 7000 MWCO, Thermo Scientific, Prod #: 21329) pre-equilibrated with 1× PBS. The 800CW was conjugated to BSA-biotin following the manufacturer's protocol for labeling high molecular weight proteins (LI-COR Biosciences, Lincoln, NE). 0.1 mL of 1 M potassium phosphate buffer (K_2HPO_4, pH = 9) was added into 1 mL of purified BSA-biotin solution to raise the pH. Next, 25 μL of 4 mg/mL NHS-800CW (Licor, 929–70020) was added to the mixture, and the solution was incubated at 23°C for 2.5 hours. Free NHS-800CW was then separated from the conjugate using a Zeba desalting column (Thermo Fisher Scientific). After purification, 800CW-BSA was collected for the FUSIN delivery. The final concentration of BSA was determined using the NanoDrop-2000 (Thermo Fisher Scientific, Wilmington, DE, USA). The collected 800CW-BSA was diluted in saline by factors of 50×, 100×, 200× and 400× and imaged by the Pearl Image System (LI-COR Biosciences, Lincoln, NE). The results verified that the fluorescence intensity of 800CW detected by the Pearl Imaging System was linearly correlated with the BSA concentration (Fig. 1F).

IN administration

The IN administration procedure was the same as reported before [32]. Mice were placed supine under anesthesia. Drops (3 μL each) of 800CW-BSA (concentration ~1.3 mg/mL) were administered to the mouse nose, alternating between the left and right nostrils every 2 mins. These drops were placed at the opening of the nostril, allowing the animal to snort each drop into the nasal cavity. A total of 8 drops (24 μL) were administered to each mouse.

FUS treatment

An ultrasound image-guided FUS system (VIFU 2000; Alpinion US Inc., Bothell, WA, USA) consisting of a FUS transducer with a center frequency of 1.5 MHz, a focal depth of 60 mm, an aperture of 60 mm, and a circular central opening of 38 mm was used in this study (Fig. 1A and 1B). The pressure amplitudes and beam profiles of the FUS transducer were calibrated using a needle hydrophone in a degassed water tank before the experiment. The reported pressure amplitudes were corrected for 18% mouse skull attenuation [57]. The axial and lateral full-width-at-half-maximum (FWHM) focal regions of the FUS transducer in the system were 6.04 mm and 0.62 mm, respectively. An ultrasound imaging probe (L8-17, working frequency 8 –17 MHz, center frequency 12 MHz, Alpinion, Seoul, Korea) was inserted into the FUS transducer center opening and aligned with the FUS focal plane.

FUS was targeted at the right side of the brainstem under the guidance of ultrasound imaging using the L8-17 probe with the assistance of a grid [58].

The animal was stabilized by a stereotaxic frame in the prone position after the IN administration to prepare for FUS treatment (Fig. 1B). The fur on the mouse head was removed, and a water container filled with degassed water was placed on the mouse head and coupled with degassed ultrasound gel for FUS coupling. The bottom of the water container had a window sealed with a transparent membrane (Tegaderm®, 3M Health Care, St. Paul, MN, USA). The FUS transducer was attached to a water balloon filled with degassed water. The water balloon was immersed in the water container to provide acoustic coupling (Fig. 1A and B). A tail vein catheter was inserted into the mouse tail vein for the injection of microbubbles. The time normally needed to finish the above mouse preparation was 0.5 hours. Size-isolated microbubbles (median diameter of 4–5 μm) manufactured in-house [59] were injected through the tail vein, and this was immediately followed by FUS sonication. FUS sonication was performed at different time points after IN administration (T_{lag1} = 0.5 h, 1.5 h, and 4.0 h) (Fig. 1D). The following FUS parameters were used: pressure = 0.43 MPa, 0.56 MPa, or 0.70 MPa, pulse length = 6.7 ms, pulse repetition frequency = 5 Hz, and duration = 1 min. Four points located at the corners of a square with a side length of 0.6 mm were treated in order to enlarge the treatment volume. Mice were transcardially-perfused at different time points post-FUS treatment (T_{lag2} = 0.5 h, 1.0 h, and 4.0 h). Mice in the control group (group 1) were perfused at ~1.0 h after IN administration of 800CW-BSA.

Ex vivo fluorescence imaging and analysis

After perfusion, the brains were excised and sliced into 2-mm coronal sections using a brain matrix (RBM-2000C; ASI Instruments, Inc., Warren, MI, USA) (Fig. 1E). The nose, trigeminal nerve, heart, lung, spleen, kidney, liver, stomach, and intestines were harvested in groups 2, 5, and 6 to study the biodistribution of 800CW-BSA at different time points. The brain slices and all organs were examined by the Pearl Imaging System using the 800 nm channel for 800CW-BSA (Fig. 1E). The Pearl Imaging System offers *in vivo* imaging in the NIR range (700 – 900 nm), where tissue autofluorescence and absorption are low. This system allows a wide dynamic range (22 bits) capture, which can image samples with fluorescence intensity of a million-fold difference and avoid saturation or underexposure [60]. The exposure time for fluorescence imaging was kept the same (30 s) for all groups. The fluorescence intensity of the brain slices and organs were quantified using LI-COR's Image Studio Lite software by an experimenter blinded to experimental conditions.

Histologic analysis

Our previous study of FUSIN delivery showed that FUS treatment at an acoustic pressure of 0.56 MPa did not cause histological damage to the mouse brainstem [33]. In this study, three different pressures (0.43 MPa, 0.56 MPa, and 0.70 MPa) were used for FUSIN treatment. We performed histologic examinations of mice treated with 0.70 MPa using hematoxylin and eosin (H&E) staining and compared with control mice without treatment (groups 1 and 8 as listed in Table 1). After fluorescence imaging of the 2-mm thick brain slices, the mouse brainstems were fixed in 4% paraformaldehyde overnight, followed by cryoprotected with

sucrose. The brainstems were sectioned coronally into 15 μm sections and stained with H&E. Histological evaluation was performed single-blinded by an observer without knowledge of the location and parameters of sonication.

Statistical analysis

Statistical analyses were performed using R statistical software v3.5.0 (https://www.R-project.org/), and figures were produced using GraphPad Prism (Version 8.3, La Jolla, CA, USA). Differences among groups were determined using a non-parametric Kruskal-Wallis test (one-way ANOVA on ranks) followed by post hoc non-parametric Mann-Whitney U tests for group-wise comparisons. P-value < 0.05 was used to determine statistical significance.

Results

Impact of the time interval between IN and FUS (T_{lag1})

Representative fluorescence images of the mouse brain slices and the corresponding quantification of 800CW-BSA fluorescence intensity in the brainstem for each group are presented in Figure 2. Among the groups treated with FUS after IN administration with different T_{lag1} and non-treated control group, there was a significant between-group difference in fluorescence intensity (n = 24; four groups; Kruskal-Wallis chi-squared = 15.1, df = 3, $p = 0.0018$). The delivery outcome of 800CW-BSA in the T_{lag1} = 0.5 h group as indicated by the measured fluorescence intensity was found to be on average 24.5-fold, 5.4-fold, and 21.6-fold higher than those in the controlled IN only, T_{lag1} = 1.5 h, and T_{lag1} = 4.0 h groups, respectively (Fig. 2B). FUS applied at 1.5 h and 4.0 h post-IN administration did not show a significant difference in the delivery outcomes when compared with IN only.

Impact of FUS pressure

A significant group effect was observed on fluorescence intensity among the FUS-treated mice with different acoustic pressures (0.43 MPa, 0.56 MPa, and 0.70 MPa) and the non-treated control mice (n = 24; four groups; Kruskal-Wallis chi-squared = 16.1, df = 3, $p = 0.0011$). Overall, the FUS-treated groups showed significantly higher fluorescence intensity compared to the mice in the IN-only group (Fig. 3). Mice treated with 0.43 MPa demonstrated 1.8-fold and 3.7-fold higher mean fluorescence intensity than those treated with 0.56 MPa and 0.70 MPa, respectively (Fig. 3B). Exploratory analysis revealed a negative correlation between the fluorescence intensity and FUS pressure (among the FUS-treated mice: n=18; Kendall tau-b correlation = −0.45, $p = 0.021$).

Impact of the sacrifice time post-FUS (T_{lag2})

Significant between-group difference in fluorescence intensity was observed (Kruskal-Wallis chi-squared = 10.2, df = 2, $p = 0.006$) among mice with different sacrifice times post-FUS (n = 18; three groups: T_{lag2} = 0.5 h, 1.0 h, and 4.0 h). The brainstem retention of 800CW-BSA was similar at T_{lag2} = 0.5 h and T_{lag2} = 1.0 h post-FUS, while at T_{lag2} = 4.0 h, the average retention of 800CW-BSA had dropped by 5.5-fold and 4.9-fold compared to at 0.5 h and 1.0 h, respectively (Fig. 4B).

Systemic exposure associated with FUSIN

Figure 5A displays representative fluorescence images of major organs, including the heart, lung, spleen, kidneys, liver, stomach, and intestines, as well as the nose and trigeminal nerve collected from mice sacrificed at the three different T_{lag2} times post-FUS. Figure 5B shows the corresponding quantification results. In terms of 800CW-BSA distribution in organs, the fluorescence signals were mainly observed in the stomach and intestines, with fluorescence intensity about two orders of magnitude higher than in other organs. The fluorescence signal was higher at 4.0 h compared to at 0.5 h and 1.0 h in the stomach and intestines. The 800CW-BSA also accumulated in the nose and trigeminal nerve; however, in contrast to the stomach and intestines, the amount of 800CW-BSA at 4.0 h was decreased by 62% and 87%, respectively, in the nose and trigeminal nerve compared to at 0.5 h.

H&E staining—Representative H&E staining of the FUS-treated side of the brainstem showed no hemorrhage or neuron damage at the highest tested acoustic pressure level (0.70 MPa) compared with the control without treatment (Fig. 6). No tissue damage was consistently observed in all the H&E-stained mouse brain slices.

Discussion

This study characterized the FUSIN brain drug delivery technique by evaluating the impact of critical experimental factors, including the time interval between IN and FUS, the FUS pressure, and the sampling time after FUS treatment. Findings from this study revealed that FUSIN delivery outcome depends on these critical experimental parameters, providing insights for selecting optimal treatment parameters, and shinning light on the potential mechanisms of FUSIN.

A previous study performed FUS either before or after the IN delivery of a fluorescently labeled dextran and found that FUS enhanced the delivery only when applied after IN, while the pretreatment by FUS followed by IN did not show significantly enhanced delivery compared with IN only. This previous finding suggested that FUS could enhance the accumulation of IN-administered agents when the agents have already existed in the FUS-targeted brain region [32]. A recent FDA approved device for enhancing transdermal delivery, Low-Frequency Sonophoresis (LSF), requires the agents to be administered after sonication. LSF utilizes the violent collapse of cavitation bubbles (*i.e.*, inertial cavitation) to produce microjets and microstreaming that can disrupt the lipid bilayers of the stratum corneum microscopically in the transdermal delivery [61]. Moreover, LSF can lead to a typical temperature increase of ~10°C [62,63]. Both inertial cavitation and the associated thermal effects may change the properties of the therapeutics; therefore, agents are administered after ultrasound sonication. However, FUSIN uses FUS with intensity at the diagnostic ultrasound range and the physical mechanism is stable cavitation as the pressure is often below inertial cavitation threshold in the mouse brain [64]. Stable cavitation is utilized instead of inertial cavitation to avoid any potential damage to the sensitive brain tissue. The gentle mechanical oscillation should have a low chance of changing the therapeutics, allowing the agents to be administered before FUS sonication. The current study performed IN followed by FUS and examined the impact of the time interval between

IN and FUS (T_{lag1}). It was found that FUSIN delivery of 800CW-BSA to the brainstem reached the greatest accumulation at 0.5 h among the three tested T_{lag1}, and decreased as T_{lag1} increased to 1.5 h and 4.0 h (Fig. 2). It was reported before that concentration of IN administerd albumin at the brainstem significantly decreased as time increased from 0.5 h to 4.0 h post-IN [40]. Combing this report and our finding, it implies that FUSIN achieves greater delivery when FUS is applied as the IN-administered agent reaches higher concentration in the targetd brain region. The T_{lag1} needs to be selected in consideration of the pharmacokinetics of the IN-delivered agents in the brain.

Although both FUSIN and FUS-BBBD are FUS-mediated brain drug delivery techniques, and both can achieve enhanced drug delivery to the targeted brain location, the correlations between their delivery efficiency and the acoustic pressure exhibit opposite trends. Based on previous reports, the efficiency of FUS-BBBD delivery mainly depends on acoustic pressure. Higher pressure is associated with a higher increase in BBB permeability and thus improved efficiency of trans-BBB delivery [1,44,65–67]. However, in this study, the amount of 800CW-BSA at the brainstem delivered by FUSIN decreased with higher FUS pressure (Fig. 3). This finding supports our hypothesis that FUSIN achieves enhanced drug delivery not by increasing the BBB permeability but through another mechanism. Our proposed “microbubble pump effect” may induce blood vessel expansion and contraction via the volumetric oscillating microbubbles, resulting in increased transport of IN-administered agents along the perivascular spaces into the brain parenchyma. The observation that lower pressure was associated with higher amount of 800CW-BSA delivered by FUSIN suggests that high acoustic pressures can potentially lead to faster disruption of microbubbles, thereby reducing the microbubble pump effect. It is also possible that FUS-induced BBB disruption could enhance “two-way trafficking” between brain and blood as suggested by our previous study, meaning that molecules in the blood circulation can enter the brain after FUS-BBBD, and meanwhile, molecules in the brain tissue can also be released into the blood circulation [68]. Thus, we also suspect that higher pressures lead to higher enhancement of BBB permeability, which may facilitate the release of 800CW-BSA from the perivascular space into the blood circulation and thus lead to decreased delivery by FUSIN at higher pressures. Although future studies are needed to better understand the mechanism of FUSIN delivery, our findings indicate that the mechanism of FUSIN delivery is different from that of FUS-BBBD.

Among the three T_{lag2} evaluated in this study, the accumulated amount of 800CW-BSA in the mouse brainstem decreased from 0.5 h to 4.0 h post-FUS (Fig. 4). This finding is in contrast to a previous study reporting increasing brain uptake of albumin FUS-BBBD over 24 h [69]. The level of 800CW-BSA in the brain parenchyma represents a balance between drug delivery into the brain and its clearance out of the brain. In FUS-BBBD delivery, since albumin has a relatively long half-life in blood circulation (~19 days) [70], it can be continuously delivered across the disrupted BBB from the blood circulation as long as the BBB remains open. The aforementioned previous study observed a continuous increase of brain uptake of albumin over 24 h after FUS-BBBD treatment, suggesting that the delivery rate of albumin across the BBB was higher than the clearance rate within this time frame [69]. Our finding that the amount of albumin delivered by FUSIN decreased over a 4.0 h time frame implies that contrary to FUS-BBBD, albumin delivered by FUSIN had a higher

clearance rate than the delivery rate over this time frame. We suspect that because the IN-administered agent was distributed in the perivascular space, its delivery into the brain parenchyma reached the maximum immediately after the application of the FUS-induced microbubble pumping effect and then decreased over time due to brain clearance. Regarding the biodistribution of FUSIN-delivered agents in different organs, our previous study showed that IN administration could deliver agents directly from the nose to the brain, minimizing systemic exposure [33]. This study verified that FUSIN delivery was associated with low systemic exposure to all major organs except the stomach and intestines (Fig. 5). Those accumulations in the stomach and intestine could be excreted through feces, leading to minimal systemic toxicity [71]. This finding is consistent with our previous study, which found that the concentration of IN-administered radiolabeled gold nanoclusters was close to zero in all major organs except the stomach and intestines [33,72]. Different IN administration techniques can affect the deposition within the nasal epithelium as well as delivery outcomes. Nasal drops, as used in this study, have been commonly used for IN administration to mice and rats [18,73]. This method has the advantage of not involving the insertion of a flexible tube into the nasal cavity [74]. Liquid drops are placed at the opening of the nostril, allowing the animal to forcefully sniff the drops into the nasal cavity and reach the posterior part of the cavity where the olfactory epithelium is located. However, it has the disadvantage that the nasal formulation can be swallowed by the animal into the digestive system, resulting in the observed accumulation of 800CW-BSA in the stomach and intestines over time. As mentioned earlier, those accumulations could potentially be excreted through feces and minimize systemic toxicity. To prevent the nasal drops from being swallowed, one solution is to seal the esophagus and insert a breathing tube into the trachea [75,76]. In clinical studies, various nasal devices, such as sprays, droppers, and nebulizers, have been designed to target the nasal formulations to the olfactory region without deposition in the lungs or esophagus [77]. This unique advantage of FUSIN in minimizing systemic exposure suggests that FUSIN has the potential to improve the treatment of a broad spectrum of brain diseases by not only enhancing therapeutic agent delivery to diseased brain sites but also substantially reducing toxicity to other organs. The high accumulation of 800CW-BSA in the nose and the trigeminal nerve was consistent with our previous study of FUSIN delivery of gold nanoparticles [33,72]. This finding confirmed that the 800CW-BSA delivery pathway was mainly via the nose-to-brain route, which was different from the blood-to-brain route used by FUS-BBBD. The decreased fluorescence intensities in the nose and trigeminal nerve suggest that 800CW-BSA was cleared from the nose and trigeminal nerve over time, which can minimize any potential toxicity of the agent to the nose and nerve tissues.

Our previous study showed that FUSIN delivery of nanoparticles did not induce any change or damage to the nasal tissue, trigeminal nerves, or the FUS-targeted brainstem [33]. In this study, we applied different FUS pressures in FUSIN treatment and performed H&E staining of the brainstems of mice treated with the highest pressure setting (0.70 MPa) and the control mice without treatment. There was no observable vascular or tissue damage at the FUS-targeted brainstem region, which confirmed that the FUS parameters used in this study were safe at the histological level.

This study had several limitations. First, 800CW-BSA was used as a model agent. Future studies are needed to compare FUSIN delivery of different agents in order to further characterize the dependence of FUSIN delivery outcomes on agent characteristics such as size, surface charge, and material. Second, the present study only showed the dependence of FUSIN on acoustic pressure. Other FUS parameters (e.g., frequency, pulse length, and pulse repetition frequency), as well as microbubble characteristics (e.g., resonant frequency, size, and shell properties), may also be related to FUSIN outcomes and should be studied in the future. Third, this study only focused on drug delivery to the brainstem. Further research is needed to assess the brain location dependency of FUSIN by comparing the delivery outcomes of the same agent to different brain locations. Fourth, the mechanism of FUSIN delivery is not clear. Further study is needed to provide direct evidence to show how FUSIN works in brain drug delivery.

Conclusion

FUSIN is a promising technique for brain drug delivery that integrates FUS and microbubbles to enhance the accumulation of intranasally administered agents at the FUS-targeted brain location. The current study found that the measured FUSIN delivery outcomes depend on several critical experimental parameters, including the time interval between IN and FUS, the FUS pressure, and the sampling time. This study revealed the unique characteristics of FUSIN as a noninvasive, efficient, and localized brain drug delivery technique with minimal systemic exposure.

Supplementary Material

Refer to Web version on PubMed Central for supplementary material.

Acknowledgments

This work was supported by the National Institutes of Health (NIH) grants R01EB027223, R01EB030102 and R01MH116981. It was also partially supported by the Charlie Teo Foundation. The authors would like to thank Yimei Yue for assisting with the animal experiment and Dr. Srikanth Singamaneni for providing the 800CW-BSA.

References

[1]. Hynynen K, McDannold N, Vykhodtseva N, Jolesz FA, Noninvasive MR imaging-guided focal opening of the blood-brain barrier in rabbits., Radiology. 220 (2001) 640–646. http://www.ncbi.nlm.nih.gov/pubmed/11526261. [PubMed: 11526261]

[2]. Chen H, Kreider W, Brayman AA, Bailey MR, Matula TJ, Blood vessel deformations on microsecond time scales by ultrasonic cavitation, Phys. Rev. Lett 106 (2011) 034301. doi:10.1103/PhysRevLett.106.034301. [PubMed: 21405276]

[3]. Park J, Aryal M, Vykhodtseva N, Zhang Y-Z, McDannold N, Evaluation of permeability, doxorubicin delivery, and drug retention in a rat brain tumor model after ultrasound-induced blood-tumor barrier disruption, J. Control. Release 250 (2017) 77–85. doi:10.1016/j.jconrel.2016.10.011. [PubMed: 27742444]

[4]. Jordão JF, Ayala-Grosso CA, Markham K, Huang Y, Chopra R, McLaurin J, Hynynen K, Aubert I, Antibodies targeted to the brain with image-guided focused ultrasound reduces amyloid-beta plaque load in the TgCRND8 mouse model of Alzheimer's disease., PLoS One. 5 (2010) e10549. doi:10.1371/journal.pone.0010549. [PubMed: 20485502]

[5]. Manabu Kinoshita N McDannold, F.A. Jolesz, Noninvasive localized delivery of Herceptin to the mouse brain by MRI-guided focused ultrasound-induced blood-brain barrier disruption., Proc. Natl. Acad. Sci. U. S. A 103 (2006) 11719–23. doi:10.1073/pnas.0604318103. [PubMed: 16868082]

[6]. Alonso A, Reinz E, Leuchs B, Kleinschmidt J, Fatar M, Geers B, Lentacker I, Hennerici MG, De Smedt SC, Meairs S, Focal delivery of AAV2/1-transgenes into the rat brain by localized ultrasound-induced BBB opening., Mol. Ther. Nucleic Acids 2 (2013) e73. doi:10.1038/mtna.2012.64. [PubMed: 23423361]

[7]. Wang S, Kugelman T, Buch A, Herman M, Han Y, Karakatsani ME, Hussaini SA, Duff K, Konofagou EE, Non-invasive, Focused Ultrasound-Facilitated Gene Delivery for Optogenetics., Sci. Rep 7 (2017) 39955. doi:10.1038/srep39955. [PubMed: 28059117]

[8]. Wang S, Olumolade OO, Sun T, Samiotaki G, Konofagou EE, Noninvasive, neuron-specific gene therapy can be facilitated by focused ultrasound and recombinant adeno-associated virus, Gene Ther. 22 (2014) 104–110. doi:10.1038/gt.2014.91. [PubMed: 25354683]

[9]. Burgess A, Ayala-Grosso CA, Ganguly M, Jordão JF, Aubert I, Hynynen K, Targeted delivery of neural stem cells to the brain using MRI-guided focused ultrasound to disrupt the blood-brain barrier., PLoS One. 6 (2011) e27877. doi:10.1371/journal.pone.0027877. [PubMed: 22114718]

[10]. Shen W-B, Anastasiadis P, Nguyen B, Yarnell D, Yarowsky PJ, Frenkel V, Fishman PS, Magnetic enhancement of stem cell–targeted delivery into the brain following MR-guided focused ultrasound for opening the blood–brain barrier, Cell Transplant. 26 (2017) 1235–1246. doi:10.1177/0963689717715824. [PubMed: 28933214]

[11]. Carpentier A, Canney M, Vignot A, Reina V, Beccaria K, Horodyckid C, Karachi C, Leclercq D, Lafon C, Chapelon JY, Capelle L, Cornu P, Sanson M, Hoang-Xuan K, Delattre JY, Idbaih A, Clinical trial of blood-brain barrier disruption by pulsed ultrasound, Sci. Transl. Med 8 (2016) 343re2–343re2. doi:10.1126/scitranslmed.aaf6086.

[12]. Park SH, Kim MJ, Jung HH, Chang WS, Choi HS, Rachmilevitch I, Zadicario E, Chang JW, Safety and feasibility of multiple blood-brain barrier disruptions for the treatment of glioblastoma in patients undergoing standard adjuvant chemotherapy, J. Neurosurg (2020) 1–9. doi:10.3171/2019.10.jns192206.

[13]. Mainprize T, Lipsman N, Huang Y, Meng Y, Bethune A, Ironside S, Heyn C, Alkins R, Trudeau M, Sahgal A, Perry J, Hynynen K, Blood-brain barrier opening in primary brain tumors with non-invasive MR-guided focused ultrasound: A clinical safety and feasibility study, Sci. Rep 9 (2019) 321. doi:10.1038/s41598-018-36340-0. [PubMed: 30674905]

[14]. Lipsman N, Meng Y, Bethune AJ, Huang Y, Lam B, Masellis M, Herrmann N, Heyn C, Aubert I, Boutet A, Smith GS, Hynynen K, Black SE, Blood–brain barrier opening in Alzheimer's disease using MR-guided focused ultrasound, Nat. Commun 9 (2018) 2336. doi:10.1038/s41467-018-04529-6. [PubMed: 30046032]

[15]. Meng Y, Abrahao A, Heyn CC, Bethune AJ, Huang Y, Pople CB, Aubert I, Hamani C, Zinman L, Hynynen K, Black SE, Lipsman N, Glymphatics visualization after focused ultrasound-induced blood–brain barrier opening in humans, Ann. Neurol 86 (2019) 975–980. doi:10.1002/ana.25604. [PubMed: 31525269]

[16]. Rezai AR, Ranjan M, D'Haese P-F, Haut MW, Carpenter J, Najib U, Mehta RI, Chazen JL, Zibly Z, Yates JR, Hodder SL, Kaplitt M, Noninvasive hippocampal blood-brain barrier opening in Alzheimer's disease with focused ultrasound, Proc. Natl. Acad. Sci (2020) 202002571. doi:10.1073/pnas.2002571117.

[17]. Abrahao A, Meng Y, Llinas M, Huang Y, Hamani C, Mainprize T, Aubert I, Heyn C, Black SE, Hynynen K, Lipsman N, Zinman L, First-in-human trial of blood-brain barrier opening in amyotrophic lateral sclerosis using MR-guided focused ultrasound., Nat. Commun 10 (2019) 4373. doi:10.1038/s41467-019-12426-9. [PubMed: 31558719]

[18]. Thorne RG, Pronk GJ, Padmanabhan V, Frey WH, Delivery of insulin-like growth factor-I to the rat brain and spinal cord along olfactory and trigeminal pathways following intranasal administration, Neuroscience. 127 (2004) 481–496. doi:10.1016/j.neuroscience.2004.05.029. [PubMed: 15262337]

[19]. Iliff JJ, Nedergaard M, Benveniste H, Iliff JJ, Lee H, Yu M, Feng T, Logan J, Nedergaard M, Benveniste H, Brain-wide pathway for waste clearance captured by contrast-enhanced MRI, J. Clin. Invest 123 (2013) 1299–1309. doi:10.1172/JCI67677.2-photon. [PubMed: 23434588]

[20]. Iliff JJ, Wang M, Liao Y, Plogg BA, Peng W, Gundersen GA, Benveniste H, Vates GE, Deane R, Goldman SA, Nagelhus EA, Nedergaard M, A paravascular pathway facilitates CSF flow through the brain parenchyma and the clearance of interstitial solutes, including amyloid β, Sci. Transl. Med 4 (2012) 147ra111. doi:10.1126/scitranslmed.3003748.

[21]. Meredith ME, Salameh TS, Banks WA, Intranasal delivery of proteins and peptides in the treatment of neurodegenerative diseases, AAPS J. 17 (2015) 780–787. doi:10.1208/s12248-015-9719-7. [PubMed: 25801717]

[22]. Zhao Y-Z, Lin M, Lin Q, Yang W, Yu X-C, Tian F-R, Mao K-L, Yang J-J, Lu C-T, Wong HL, Intranasal delivery of bFGF with nanoliposomes enhances in vivo neuroprotection and neural injury recovery in a rodent stroke model, J. Control. Release 224 (2016) 165–175. doi:10.1016/j.jconrel.2016.01.017. [PubMed: 26774220]

[23]. Kim I-D, Shin J-H, Kim S-W, Choi S, Ahn J, Han P-L, Park J-S, Lee J-K, Intranasal delivery of HMGB1 siRNA confers target gene knockdown and robust neuroprotection in the postischemic brain, Mol. Ther 20 (2012) 829–839. doi:10.1038/mt.2011.291. [PubMed: 22252450]

[24]. Rodriguez M, Lapierre J, Ojha CR, Kaushik A, Batrakova E, Kashanchi F, Dever SM, Nair M, El-Hage N, Intranasal drug delivery of small interfering RNA targeting Beclin1 encapsulated with polyethylenimine (PEI) in mouse brain to achieve HIV attenuation., Sci. Rep 7 (2017) 1862. doi:10.1038/s41598-017-01819-9. [PubMed: 28500326]

[25]. Sekerdag E, Lüle S, Bozdağ Pehlivan S, Öztürk N, Kara A, Kaffashi A, Vural I, Işıkay I, Yavuz B, Oguz KK, Söylemezoğlu F, Gürsoy-Özdemir Y, Mut M, A potential non-invasive glioblastoma treatment: Nose-to-brain delivery of farnesylthiosalicylic acid incorporated hybrid nanoparticles, J. Control. Release 261 (2017) 187–198. doi:10.1016/j.jconrel.2017.06.032. [PubMed: 28684169]

[26]. Rassu G, Soddu E, Posadino AM, Pintus G, Sarmento B, Giunchedi P, Gavini E, Nose-to-brain delivery of BACE1 siRNA loaded in solid lipid nanoparticles for Alzheimer's therapy, Colloids Surfaces B Biointerfaces. 152 (2017) 296–301. doi:10.1016/j.colsurfb.2017.01.031. [PubMed: 28126681]

[27]. Wu S, Li K, Yan Y, Gran B, Han Y, Zhou F, Guan Y-T, Rostami A, Zhang G-X, Intranasal delivery of neural stem cells: A CNS-specific, non-invasive cell-based therapy for experimental autoimmune encephalomyelitis., J. Clin. Cell. Immunol 4 (2013). doi:10.4172/2155-9899.1000142.

[28]. Freiherr J, Hallschmid M, Frey II WH, Brünner YF, Chapman CD, Hölscher C, Craft S, De Felice FG, Benedict C, Intranasal insulin as a treatment for Alzheimer's disease: a review of basic research and clinical evidence., CNS Drugs. 27 (2013) 505–14. doi:10.1007/s40263-013-0076-8. [PubMed: 23719722]

[29]. Illum L, Nasal drug delivery - Possibilities, problems and solutions, J. Control. Release 87 (2003) 187–198. doi:10.1016/S0168-3659(02)00363-2. [PubMed: 12618035]

[30]. Kozlovskaya L, Abou-Kaoud M, Stepensky D, Quantitative analysis of drug delivery to the brain via nasal route., J. Control. Release 189C (2014) 133–140. doi:10.1016/j.jconrel.2014.06.053.

[31]. Chen H, Chen CC, Acosta C, Wu S-Y, Sun T, Konofagou EE, A new brain drug delivery strategy: Focused ultrasound-enhanced intranasal drug delivery, PLoS One. 9 (2014) e108880. doi:10.1371/journal.pone.0108880. [PubMed: 25279463]

[32]. Chen H, Yang GZX, Getachew H, Acosta C, Sierra Sánchez C, Konofagou EE, Focused ultrasound-enhanced intranasal brain delivery of brain-derived neurotrophic factor, Sci. Rep 6 (2016) 28599. doi:10.1038/srep28599. [PubMed: 27345430]

[33]. Ye D, Zhang X, Yue Y, Raliya R, Biswas P, Taylor S, Tai Y, Rubin JB, Liu Y, Chen H, Focused ultrasound combined with microbubble-mediated intranasal delivery of gold nanoclusters to the brain, J. Control. Release 286 (2018) 145–153. doi:10.1016/j.jconrel.2018.07.020. [PubMed: 30009893]

[34]. Ji R, Smith M, Niimi Y, Karakatsani ME, Murillo MF, Jackson-Lewis V, Przedborski S, Konofagou EE, Focused ultrasound enhanced intranasal delivery of brain derived neurotrophic

factor produces neurorestorative effects in a Parkinson's disease mouse model, Sci. Rep 9 (2019) 19402. doi:10.1038/s41598-019-55294-5. [PubMed: 31852909]

[35]. Chen H, Li X, Wan M, Wang S, High-speed observation of cavitation bubble clouds near a tissue boundary in high-intensity focused ultrasound fields, Ultrasonics. 49 (2009) 289–292. doi:10.1016/j.ultras.2008.09.010. [PubMed: 19041998]

[36]. Grade S, Eberhard J, Neumeister A, Wagener P, Winkel A, Stiesch M, Barcikowski S, Serum albumin reduces the antibacterial and cytotoxic effects of hydrogel-embedded colloidal silver nanoparticles, RSC Adv. 2 (2012) 7190. doi:10.1039/c2ra20546g.

[37]. T'jollyn H, Vermeulen A, Van Bocxlaer J, Colin P, A Physiologically Based Pharmacokinetic Perspective on the Clinical Utility of Albumin-Based Dose Adjustments in Critically Ill Patients, Clin. Pharmacokinet 57 (2018) 59–69. doi:10.1007/s40262-017-0549-x. [PubMed: 28497260]

[38]. Hawkins BT, Egleton RD, Fluorescence imaging of blood-brain barrier disruption, J. Neurosci. Methods 151 (2006) 262–267. doi:10.1016/j.jneumeth.2005.08.006. [PubMed: 16181683]

[39]. Michalski D, Grosche J, Pelz J, Schneider D, Weise C, Bauer U, Kacza J, Gärtner U, Hobohm C, Härtig W, A novel quantification of blood-brain barrier damage and histochemical typing after embolic stroke in rats, Brain Res. 1359 (2010) 186–200. doi:10.1016/j.brainres.2010.08.045. [PubMed: 20732314]

[40]. Falcone J. a, Salameh TS, Yi X, Cordy BJ, Mortell WG, V Kabanov A, Banks W. a, Intranasal administration as a route for drug delivery to the brain: Evidence for a unique pathway for albumin., J. Pharmacol. Exp. Ther 98108 (2014) 54–60. doi:10.1124/jpet.114.216705.

[41]. Bader KB, Holland CK, Gauging the likelihood of stable cavitation from ultrasound contrast agents., Phys. Med. Biol 58 (2013) 127–44. doi:10.1088/0031-9155/58/1/127. [PubMed: 23221109]

[42]. Chu PC, Chai W-Y, Tsai C-H, Kang S-T, Yeh C-K, Liu H-L, Focused ultrasound-induced blood-brain barrier opening: Association with mechanical index and cavitation index analyzed by dynamic contrast-enhanced magnetic-resonance imaging., Sci. Rep 6 (2016) 33264. doi:10.1038/srep33264. [PubMed: 27630037]

[43]. Tung Y-S, Vlachos F, Feshitan JA, Borden MA, Konofagou EE, The mechanism of interaction between focused ultrasound and microbubbles in blood-brain barrier opening in mice., J. Acoust. Soc. Am 130 (2011) 3059–67. doi:10.1121/1.3646905. [PubMed: 22087933]

[44]. Chen H, Konofagou EE, The size of blood-brain barrier opening induced by focused ultrasound is dictated by the acoustic pressure, J. Cereb. Blood Flow Metab 34 (2014) 1197–204. doi:10.1038/jcbfm.2014.71. [PubMed: 24780905]

[45]. Shen Y, Guo J, Chen G, Chin CT, Chen X, Chen J, Wang F, Chen S, Dan G, Delivery of Liposomes with Different Sizes to Mice Brain after Sonication by Focused Ultrasound in the Presence of Microbubbles, Ultrasound Med. Biol (2016) 1–13. doi:10.1016/j.ultrasmedbio.2016.01.019.

[46]. Aryal M, Park J, Vykhodtseva N, Zhang Y-Z, McDannold N, Enhancement in blood-tumor barrier permeability and delivery of liposomal doxorubicin using focused ultrasound and microbubbles: evaluation during tumor progression in a rat glioma model, Phys. Med. Biol 60 (2015) 2511–2527. doi:10.1088/0031-9155/60/6/2511. [PubMed: 25746014]

[47]. Choi JJ, Selert K, Gao Z, Samiotaki G, Baseri B, Konofagou EE, Noninvasive and localized blood-brain barrier disruption using focused ultrasound can be achieved at short pulse lengths and low pulse repetition frequencies., J. Cereb. Blood Flow Metab 31 (2011) 725–737. doi:10.1038/jcbfm.2010.155. [PubMed: 20842160]

[48]. Alli S, Figueiredo CA, Golbourn B, Sabha N, Wu MY, Bondoc A, Luck A, Coluccia D, Maslink C, Smith C, Wurdak H, Hynynen K, O'Reilly M, Rutka JT, Brainstem blood brain barrier disruption using focused ultrasound: A demonstration of feasibility and enhanced doxorubicin delivery, J. Control. Release 281 (2018) 29–41. doi:10.1016/j.jconrel.2018.05.005. [PubMed: 29753957]

[49]. Mahesh S, Tang KC, Raj M, Amide bond activation of biological molecules, Molecules. 23 (2018). doi:10.3390/molecules23102615.

[50]. Davies-Venn CA, Angermiller B, Wilganowski N, Ghosh P, Harvey BR, Wu G, Kwon S, Aldrich MB, Sevick-Muraca EM, Albumin-Binding Domain Conjugate for Near-Infrared Fluorescence

Lymphatic Imaging, Mol. Imaging Biol 14 (2012) 301–314. doi:10.1007/s11307-011-0499-x. [PubMed: 21688052]

[51]. Warram JM, De Boer E, Korb M, Hartman Y, Kovar J, Markert JM, Gillespie GY, Rosenthal EL, Fluorescence-guided resection of experimental malignant glioma using cetuximab-IRDye 800CW, Br. J. Neurosurg 29 (2015) 850–858. doi:10.3109/02688697.2015.1056090. [PubMed: 26073144]

[52]. Rosenthal EL, Moore LS, Tipirneni K, De Boer E, Stevens TM, Hartman YE, Carroll WR, Zinn KR, Warram JM, Personalized Medicine and Imaging Sensitivity and Specificity of Cetuximab-IRDye800CW to Identify Regional Metastatic Disease in Head and Neck Cancer, (2017). doi:10.1158/1078-0432.CCR-16-2968.

[53]. Heuveling DA, Visser GWM, De Groot M, De Boer JF, Baclayon M, Roos WH, Wuite GJL, Leemans CR, De Bree R, Van Dongen GAMS, Nanocolloidal albumin-IRDye 800CW: A near-infrared fluorescent tracer with optimal retention in the sentinel lymph node, Eur. J. Nucl. Med. Mol. Imaging 39 (2012) 1161–1168. doi:10.1007/s00259-012-2080-5. [PubMed: 22349719]

[54]. Ter Weele EJ, Terwisscha Van Scheltinga AGT, Linssen MD, Nagengast WB, Lindner I, Jorritsma-Smit A, De Vries EGE, Kosterink JGW, Lub-De Hooge MN, Development, preclinical safety, formulation, and stability of clinical grade bevacizumab-800CW, a new near infrared fluorescent imaging agent for first in human use, Eur. J. Pharm. Biopharm 104 (2016) 226–234. doi:10.1016/j.ejpb.2016.05.008. [PubMed: 27179587]

[55]. Leung K, IRDye 800CW-Epidermal growth factor, in: Mol. Imaging Contrast Agent Database, National Center for Biotechnology Information (US), Bethesda (MD), 2004.

[56]. Kazazi-Hyseni F, Van Vuuren SH, Van Der Giezen DM, Pieters EH, Ramazani F, Rodriguez S, Veldhuis GJ, Goldschmeding R, Van Nostrum CF, Hennink WE, Kok RJ, Release and pharmacokinetics of near-infrared labeled albumin from monodisperse poly(D,L-lactic-co-hydroxymethyl glycolic acid) microspheres after subcapsular renal injection, Acta Biomater. 22 (2015) 141–154. doi:10.1016/j.actbio.2015.04.030. [PubMed: 25929814]

[57]. Choi JJ, Pernot M, Small SA, Konofagou EE, Noninvasive, transcranial and localized opening of the blood-brain barrier using focused ultrasound in mice, Ultrasound Med. Biol 33 (2007) 95–104. http://www.ncbi.nlm.nih.gov/pubmed/17189051. [PubMed: 17189051]

[58]. Sultan D, Ye D, Heo GS, Zhang X, Luehmann H, Yue Y, Detering L, Komarov S, Taylor S, Tai YC, Rubin JB, Chen H, Liu Y, Focused ultrasound enabled trans-blood brain barrier delivery of gold nanoclusters: Effect of surface charges and quantification using positron emission tomography, Small. 14 (2018) 1–9. doi:10.1002/smll.201703115.

[59]. Feshitan J. a, Chen CC, Kwan JJ, Borden M. a, Microbubble size isolation by differential centrifugation., J. Colloid Interface Sci 329 (2009) 316–24. doi:10.1016/j.jcis.2008.09.066. [PubMed: 18950786]

[60]. Liu K, Wang Y, Kong X, Liu X, Zhang Y, Tu L, Validation V, Probes O, Fluorescent N, Leblond F, Ovanesyan Z, Davis SC, Valdés PA, Kim A, Hartov A, Wilson BC, Pogue BW, Paulsen KD, Roberts DW, Miller JP, Maji D, Lam J, Tromberg BJ, Achilefu S, Liu K, Wang Y, Kong X, Liu X, Zhang Y, Tu L, Ding Y, Aalders MCG, Buma WJ, Zhang H, Wirth D, Kolste K, Kanick S, Roberts DW, Leblond F, Paulsen KD, Swartling J, Svensson J, Bengtsson D, Terike K, Andersson-Engels S, Pearl Trilogy, Biomed. Opt. Express 8 (2017) 3095. doi:10.1364/BOE.8.003656. [PubMed: 28663929]

[61]. Tezel A, Mitragotri S, Interactions of Inertial Cavitation Bubbles with Stratum Corneum Lipid Bilayers during Low-Frequency Sonophoresis, Biophys. J 85 (2003) 3502–3512. doi:10.1016/S0006-3495(03)74770-5. [PubMed: 14645045]

[62]. Tezel A, Sens A, Mitragotri S, Description of transdermal transport of hydrophilic solutes during low-frequency sonophoresis based on a modified porous pathway model, J. Pharm. Sci 92 (2003) 381–393. doi:10.1002/jps.10299. [PubMed: 12532387]

[63]. Tezel A, Dokka S, Kelly S, Hardee GE, Mitragotri S, Topical Delivery of Anti-sense Oligonucleotides Using Low-Frequency Sonophoresis, 2004.

[64]. Chen H, Konofagou EE, The size of blood-brain barrier opening induced by focused ultrasound is dictated by the acoustic pressure, J. Cereb. Blood Flow Metab 34 (2014) 1197–204. doi:10.1038/jcbfm.2014.71. [PubMed: 24780905]

[65]. Park J, Zhang Y, Vykhodtseva N, Jolesz FA, McDannold NJ, The kinetics of blood brain barrier permeability and targeted doxorubicin delivery into brain induced by focused ultrasound., J. Control. Release 162 (2012) 134–142. doi:10.1016/j.jconrel.2012.06.012. [PubMed: 22709590]

[66]. Tung Y-S, Choi JJ, Baseri B, Konofagou EE, Identifying the inertial cavitation threshold and skull effects in a vessel phantom using focused ultrasound and microbubbles., Ultrasound Med. Biol 36 (2010) 840–52. doi:10.1016/j.ultrasmedbio.2010.02.009. [PubMed: 20420973]

[67]. Xu S, Ye D, Wan L, Shentu Y, Yue Y, Wan M, Chen H, Correlation between brain tissue damage and inertial cavitation dose quantified using passive cavitation imaging, Ultrasound Med. Biol 45 (2019) 2758–2766. doi:10.1016/j.ultrasmedbio.2019.07.004. [PubMed: 31378549]

[68]. Zhu L, Cheng G, Ye D, Nazeri A, Yue Y, Liu W, Wang X, Dunn GP, Petti AA, Leuthardt EC, Chen H, Focused ultrasound-enabled brain tumor liquid biopsy, Sci. Rep 8 (2018) 6553. doi:10.1038/s41598-018-24516-7. [PubMed: 29700310]

[69]. Alonso A, Reinz E, Fatar M, Hennerici MG, Meairs S, Clearance of albumin following ultrasound-induced blood-brain barrier opening is mediated by glial but not neuronal cells., Brain Res. 1411 (2011) 9–16. doi:10.1016/j.brainres.2011.07.006. [PubMed: 21820103]

[70]. Feng J, Zhao C, Wang L, Qu L, Zhu H, Yang Z, An G, Tian H, Shou C, Development of a novel albumin-based and maleimidopropionic acid-conjugated peptide with prolonged half-life and increased in vivo anti-tumor efficacy, Theranostics. 8 (2018) 2094–2106. doi:10.7150/thno.22069. [PubMed: 29721065]

[71]. Talegaonkar S, Mishra PR, Intranasal delivery : An approach to bypass the blood brain barrier, Indian J Pharmacol 36 (2004) 140–147. doi:10.1186/1471-2202-9-S3-S5.

[72]. Ye D, Zhuang X, Yue Y, Taylor S, Tai YC, Rubin JB, Liu Y, Chen H, Comparison of Focused Ultrasound-Mediated Intranasal Delivery and Focused Ultrasound-Induced Blood-Brain Barrier Disruption in the Delivery of Gold Nanoclusters to the Brainstem, IEEE Int. Ultrason. Symp. IUS. 2018-Janua (2018) 5–8. doi:10.1109/ULTSYM.2018.8580097.

[73]. Capsoni S, Giannotta S, Cattaneo A, Nerve growth factor and galantamine ameliorate early signs of neurodegeneration in anti-nerve growth factor mice., Proc. Natl. Acad. Sci. U. S. A 99 (2002) 12432–7. doi:10.1073/pnas.192442999. [PubMed: 12205295]

[74]. Sherry Chow HH, Anavy N, Villalobos A, Direct nose-brain transport of benzoylecgonine following intranasal administration in rats, J. Pharm. Sci 90 (2001) 1729–1735. doi:10.1002/jps.1122. [PubMed: 11745730]

[75]. Hirase H, Creso J, Singleton M, Barthó P, Buzsáki G, Two-photon imaging of brain pericytes in vivo using dextran-conjugated dyes., Glia. 46 (2004) 95–100. doi:10.1002/glia.10295. [PubMed: 14999817]

[76]. Dhuria HV, Hanson LR, Frey WH, Intranasal delivery to the central nervous System: Mechanisms and experimental considerations, Int. J. Drug Dev. Res 3 (2011) 26–33. doi:10.1002/jps.

[77]. Djupesland P, Nasal drug delivery devices: characteristics and performance in a clinical perspective-a review., Drug Deliv. Transl. Res 3 (2013) 42–62. doi:10.1007/s13346-012-0108-9. [PubMed: 23316447]

- FUS-mediated intranasal delivery (FUSIN) is a promising brain drug delivery method
- FUSIN enhanced the delivery of bovine serum albumin (BSA) at the mouse brainstem
- The accumulation of BSA was low in all major organs except stomach and intestines
- FUSIN delivery outcome was affected by key experimental parameters

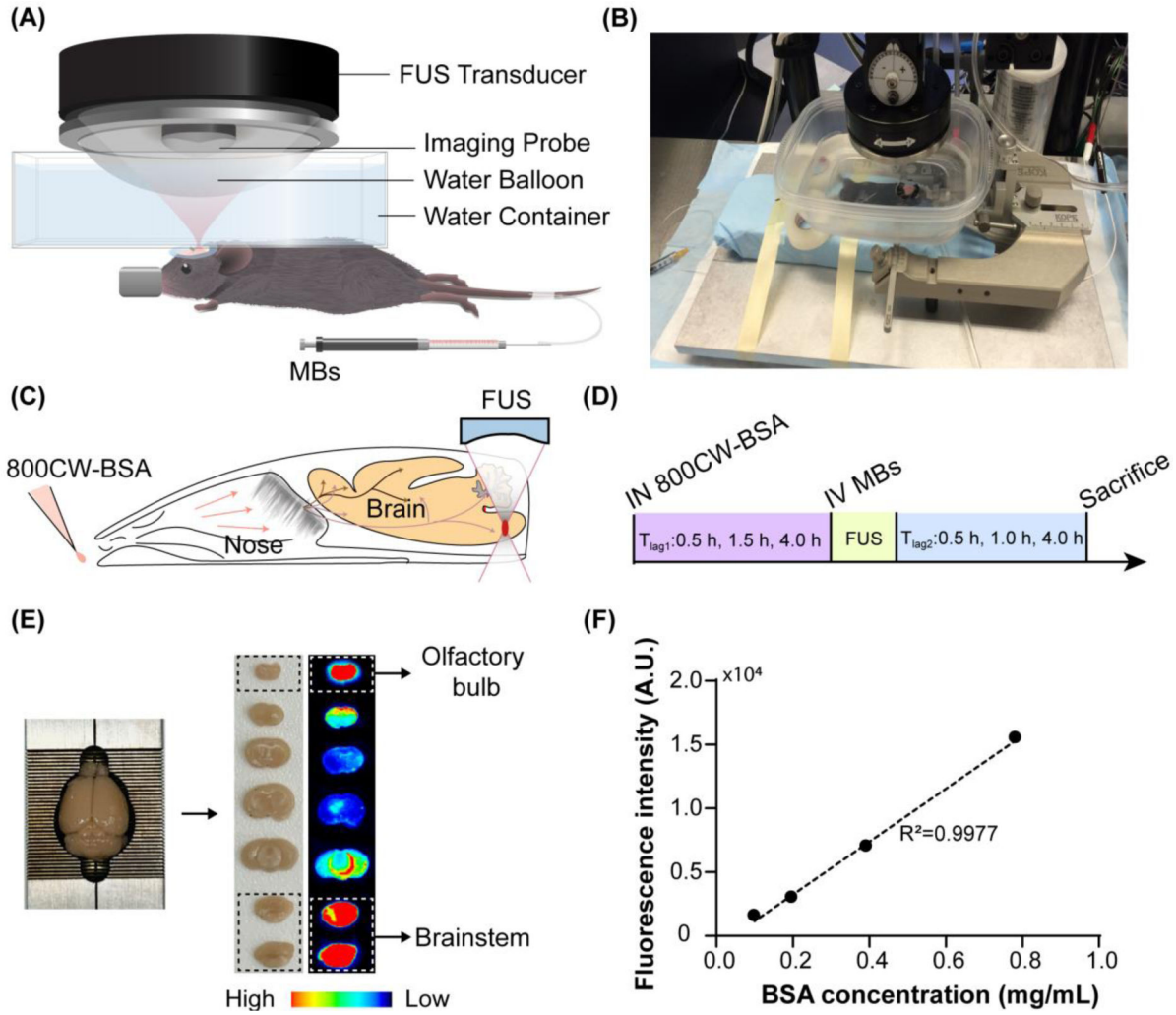

Figure 1.

Experimental methods. (A) A schematic and (B) picture of the FUS system for mouse brain treatment. Illustration of the (C) FUSIN procedure and (D) experimental timeline. IN delivery of 800CW-BSA was followed by FUS treatment targeting at the brainstem. (E) After FUSIN treatment, the mouse brain was harvested and cut into 2-mm coronal slices for fluorescence imaging. The high fluorescence intensity observed at the olfactory bulb confirmed that IN-administered 800CW-BSA transport to the brain along the olfactory pathway. (F) 800CW-BSA fluorescence intensity at different dilutions showed a linear relationship between fluorescence intensity and the concentration of 800CW-BSA.

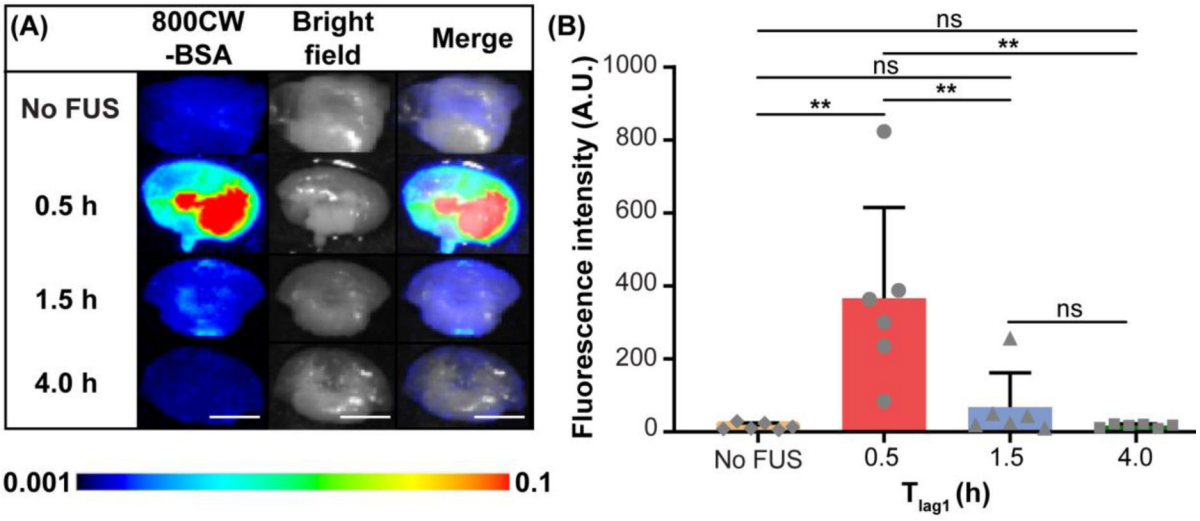

Figure 2.

FUSIN delivery of 800CW-BSA to the brainstem at different time intervals between IN and FUS (T_{lag1}) (groups 1, 2, 3, and 4 in Table 1). (A) Fluorescence images, bright field images, and their overlays of representative ex vivo mouse brainstem slices at different T_{lag1}. (B) Quantification of the 800CW-BSA fluorescence intensity at the brainstem for groups with different T_{lag1} and the control (IN only) group without FUS (Mann–Whitney U test; **: $P < 0.01$;ns: not significant). The scale bar is 5 mm.

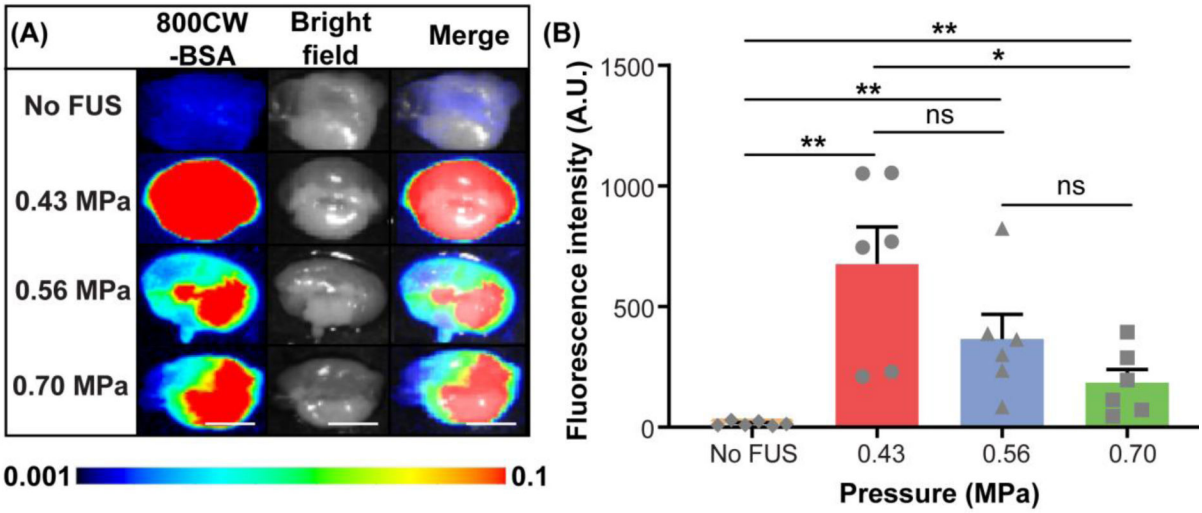

Figure 3.

FUSIN delivery of 800CW-BSA to the brainstem at different FUS pressure levels (groups 1, 2, 7, and 8 in Table 1). (A) Fluorescence images, bright field images, and their overlays of representative ex vivo mouse brain slices of the brainstem at different pressure levels. (B) Quantification of the 800CW-BSA fluorescence intensity for different pressure groups and the control (IN only) group without FUS (Mann–Whitney U test; *: $P < 0.05$; **: $P < 0.01$; ns: not significant). The scale bar is 5 mm.

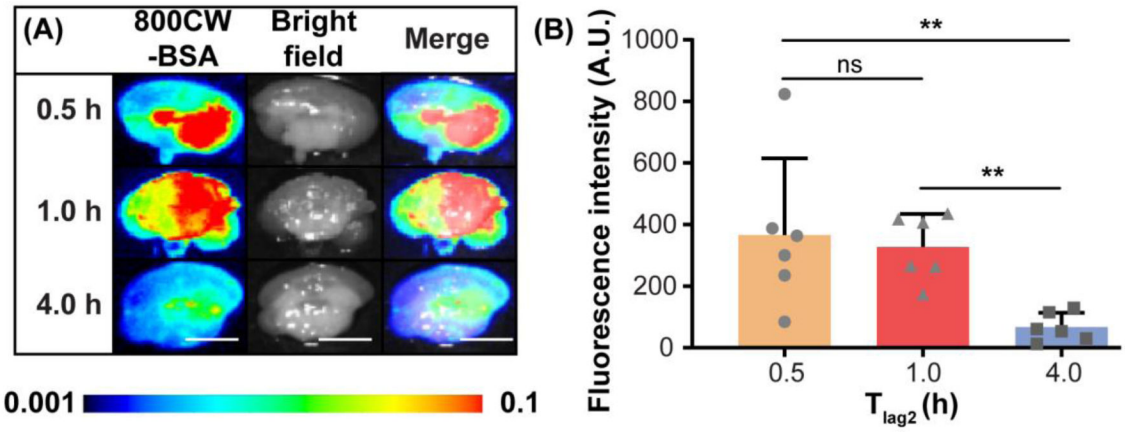

Figure 4.

The pharmacokinetics of FUSIN-delivered 800CW-BSA at the brainstem (groups 2, 5, and 6 in Table 1). (A) Fluorescence images, bright field images, and their overlays of representative ex vivo mouse brain slices at the brainstem of mice sacrificed at different T_{lag2}. (B) Quantification of the 800CW-BSA fluorescence intensity for different T_{lag2} groups (Mann–Whitney U test; **: $P < 0.01$; ns: not significant). The scale bar is 5 mm.

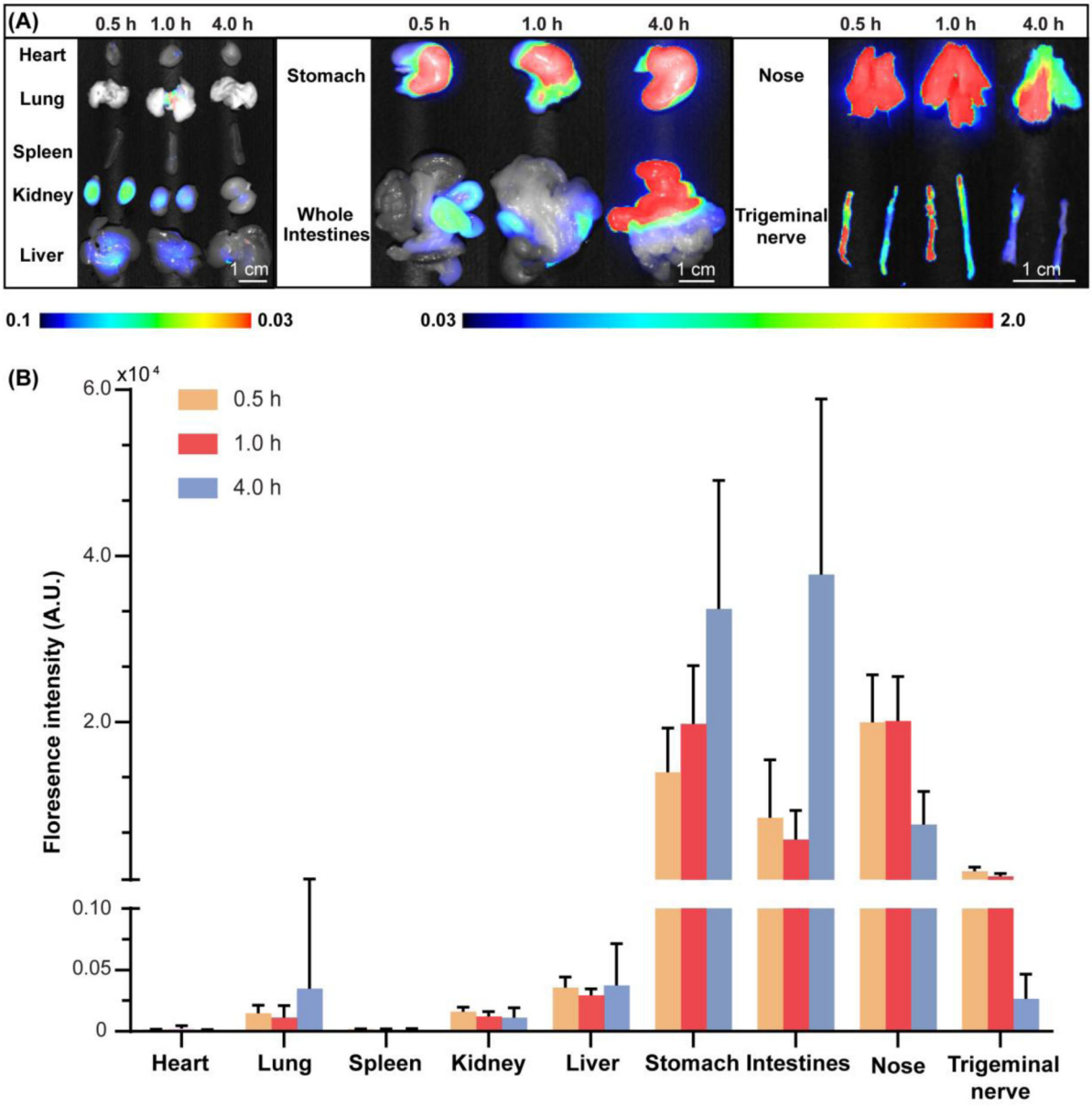

Figure 5.

The biodistribution and kinetics of 800CW-BSA delivered by FUSIN (groups 2, 5, and 6 in Table 1). (A) Fluorescence images of major organs, nose, and the trigeminal nerve at different T_{lag2}. (B) Quantification of 800CW fluorescence intensities in major organs, nose, and the trigeminal nerve at different T_{lag2}.

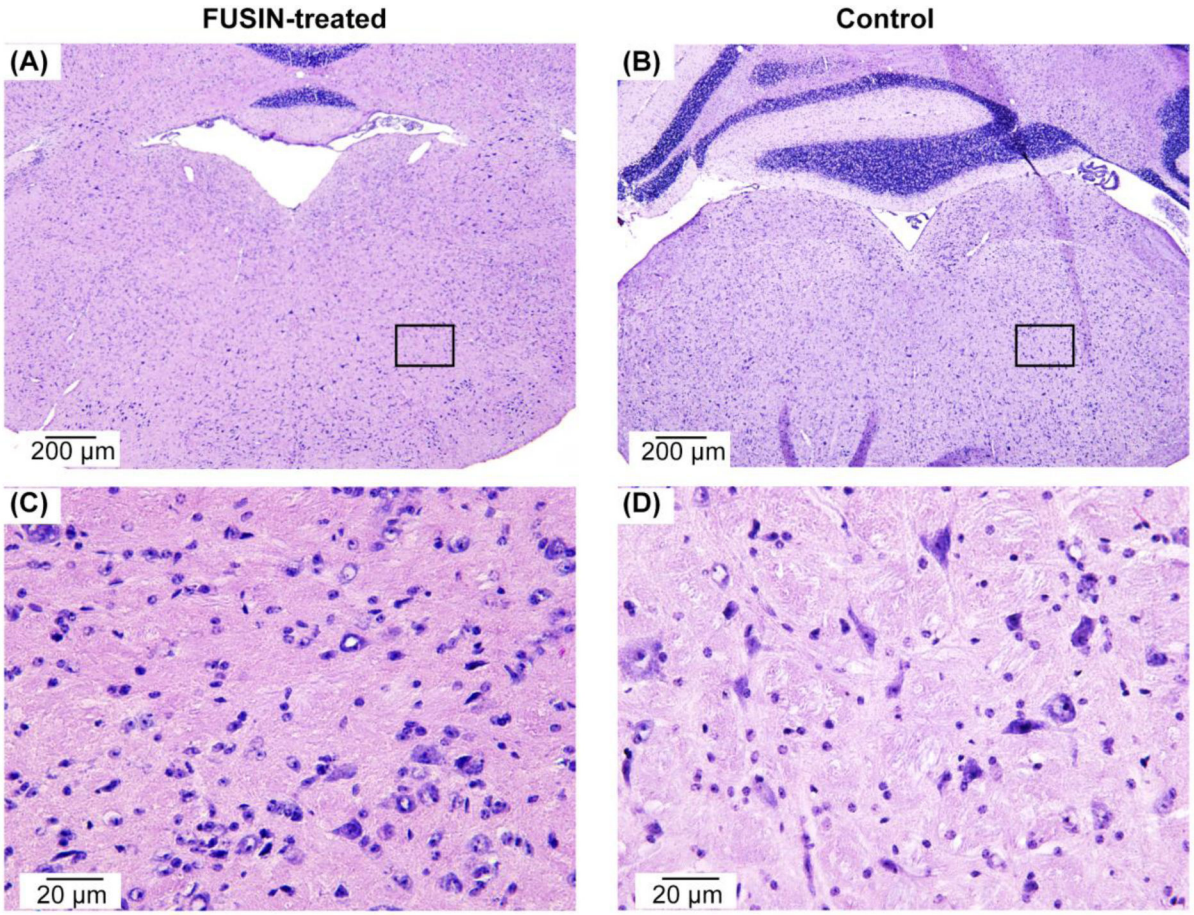

Figure 6.

Representative histological examination of the brainstems of (A) FUSIN-treated mouse at 0.70 MPa (group 8 in Table 1) and (B) non-treated control mouse (group 1 in Table 1), showing that FUSIN treatment did not induce hemorrhage or neuron damage. (C) and (D) are the zoomed-in views of the regions labeled with the boxes in (A) and (B), respectively.

Table 1.

Summary of all study groups.

Group #	Animal #	T_{lag1}	Pressure	T_{lag2}
1	6		Control (IN only)	
2	6	0.5 h	0.56 MPa	0.5 h
3	6	1.5 h	0.56 MPa	0.5 h
4	6	4.0 h	0.56 MPa	0.5 h
5	6	0.5 h	0.56 MPa	1.0 h
6	6	0.5 h	0.56 MPa	4.0 h
7	6	0.5 h	0.43 MPa	0.5 h
8	6	0.5 h	0.70 MPa	0.5 h

T_{lag1}: Time delay between IN and FUS; T_{lag2}: Time of sacrifice after FUS